


Molecular dynamics studies of $\langle a \rangle$ -type screw dislocation core structure polymorphism in titanium

Max Poschmann , Ian S. Winter ,* Mark Asta,[†] and D. C. Chrzan [‡]

Department of Materials Science and Engineering, University of California, Berkeley, California 94720, USA

 (Received 8 January 2020; revised 17 September 2021; accepted 27 October 2021; published 7 January 2022)

The atomic scale computation of dislocation core structures has become an essential tool in the development of models for the plasticity of metals. Competing dislocation core structures are often analyzed at $T = 0$ K (with T the temperature), and the dislocation core structure with the lowest energy is assumed to be the structure dictating the dynamics of the individual dislocation at finite temperatures. It is shown here that, for some hexagonal-close-packed (HCP) metals, this approach may be too simplistic. As a prototypical example, $\langle a \rangle$ -type screw dislocations within HCP Ti modeled using an empirical interatomic potential are considered. It is shown using molecular dynamics simulations that, at room temperature and above, the core structure of the dislocation is remarkably complex and variable. The implications of this complexity for the dynamics of the dislocations are discussed.

DOI: [10.1103/PhysRevMaterials.6.013603](https://doi.org/10.1103/PhysRevMaterials.6.013603)

I. INTRODUCTION

Dislocation core spreading and the resulting effects on slip were first introduced by Peierls [1] and expanded upon by Nabarro [2]. According to their model, for a given Burgers vector, line direction, and material there is a plane in which the dislocation will spread and have a minimal barrier to slip. For a dislocation with edge character this plane will always be the plane that contains both the Burgers vector and line direction, but for a pure screw dislocation these directions are parallel and thus there are many possible glide planes.

Following the introduction of the dislocation core spreading concept, there has been much work done to assess the core configurations of dislocations within various materials, including body-centered-cubic (BCC) [3–8], face-centered-cubic (FCC) [9], and hexagonal-close-packed (HCP) [10–16] metals. Thus far, the discussion of dislocation core structures has focused mostly on relaxed core structures at $T = 0$ K (with T the temperature). While it is no doubt important – not to mention surprisingly complicated – to gain an understanding of the potential energy landscape for dislocation core structures at $T = 0$ K, these core structures may not define the behavior of dislocations at finite temperatures. Specifically, the differences in energy between different core structure configurations at 0 K can be very small; e.g., for cores in HCP Ti prismatic and pyramidal spread cores differ in energy on the order of 10–20 meV/ b with b the magnitude of the Burgers vector [13,17]. Given that such energy differences are comparable to thermal energy scales on a per atom basis, it is reasonable to consider

what effects temperature may have on the core structures. (See Ref. [18] for a simple thermodynamic model of the core configurations.)

A priori, one expects that the stable core structure will be determined to be that which minimizes the excess Gibbs free energy due to the dislocation. There are many factors that can contribute to this excess free energy. For example, the dislocation will alter the phonon spectrum of the crystal, and this will lead to changes in the excess free energy. This has been argued to have a stabilizing effect on the double period reconstruction in the 90° partial dislocation in Si [19]. In the case of dissociated dislocations, the temperature dependence of the elastic constants and stacking fault energies can, in principle, alter the observed dislocation dissociation, though this effect appears to be negligible in Al [20] near room temperature. Thermal fluctuations in the position of the dislocation on the slip plane can also make a significant contribution to the excess free energy of the dislocation [21], and studies of these fluctuations have provided remarkable insight into the properties of dislocations.

This paper, however, focuses on a configurational contribution to the excess free energy of the $\langle a \rangle$ -type dislocations in hexagonal close packed (HCP) metals: the potential for a formally undissociated dislocation core to exist in multiple configurations, a property that we refer to as polymorphic dislocation core spreading.

There are many examples of polymorphic dislocation core spreading in the literature. In BCC metals, Vittek has identified nearly a continuum of dislocation core structures that can be stabilized through the application of non-Schmid stresses [6,7]. In diamond cubic semiconductors, some dislocation cores are predicted to reconstruct [19,22–25], and it is expected that the associated dislocation dynamics will be dictated by equilibrium and nonequilibrium core configurations [26]. More recently, the structure of dislocation cores within HCP metals has been studied in detail [12–16,27,28],

*ian.winter@berkeley.edu

[†]mdasta@berkeley.edu

[‡]dchrzan@berkeley.edu

and here, too, there are numerous core structures that might be observed.

As a concrete example, consider the cases of pure Ti and pure Zr. Clouet *et al.* argued that the differences in individual $\langle a \rangle$ -type screw dislocation dynamics is a result of the fact that the dislocations in the two systems assume different ground state core spreading morphologies [13]. In Ti, the dislocation cores spread slightly on the first-order pyramidal planes at $T = 0$ K, whereas in Zr, the dislocations spread slightly on the prism planes at $T = 0$ K. In both cases, the prism plane is the primary slip plane. In the case of Ti, this spread core configuration leads to thermally activated slip of the dislocations on the prism plane through a locking-unlocking mechanism [13,29,30], and results in a “jerky” motion when observed using *in situ* transmission electron microscopy. In contrast, the motion of Zr dislocations on the prism plane is much more sluggish, but smooth. Clouet *et al.* explain that the dislocations in Zr need no thermal activation because they are spread on the prism planes in their ground state.

Clouet *et al.* base their conclusions on dislocation structure calculations of the energy difference between the pyramidal and prism dislocation cores. For the case of Ti, the pyramidal spread core is found to be approximately 20 meV/ b lower in energy than the prism spread core. This energy difference is quite small. In fact, it appears to be of the order of thermal fluctuations expected in the system [18]. Moreover, the energy difference is so small that it must be approaching the limits of the accuracy of density functional theory (DFT)-based methods. Notwithstanding these observations, the predictions from the model do agree well with available experimental data, and the given explanation is certainly plausible.

However, given the small energy difference between the two core structures, one expects, at finite temperatures, to find along a single dislocation domains that appear to be spread primarily on the pyramidal plane, and domains that appear to be spread primarily on the prism plane. The numbers and sizes of these domains are expected to depend on the free energy difference between the different core states, the free energy cost associated with transitioning from one core structure to the other, and the configurational entropy contribution arising from the different configurations of core spreadings accessible to the dislocation.

In what follows, the thermal properties of these dislocation cores are studied in detail using molecular dynamics simulations. α -Ti modeled using a MEAM potential [31] is used as a prototypical system, in part due to the fact that non-Schmid stresses can be used to select either a pyramidal core or prism core as the $T = 0$ K ground state [32]. Therefore, by applying non-Schmid stresses, we can study HCP metals that behave more like Zr, and those that behave more like Ti. It is demonstrated that the structure of the dislocation core displays substantial stress-state-dependent fluctuations, even at modest temperatures. It is also demonstrated that these fluctuations have strong implications for the $\langle a \rangle$ -type screw dislocation dynamics in HCP metals, and consequently, the mechanical properties of these same metals.

In the next section of this paper, a method for assessing the core spreading tendencies of $\langle a \rangle$ -type screw dislocations in hcp metals is introduced. The section following that presents the results and discussion of molecular dynamics simulations

of $\langle a \rangle$ -type screw dislocations in α -Ti, and the final section presents the conclusions.

II. AUTOMATED IDENTIFICATION OF CORE SPREADING

The most common method for describing the core structure of a segment of dislocation within an atomic scale simulation is to calculate the Nye tensor [33] and/or the differential displacement map [6], examine the data by eye, and then make a determination of the dislocation core spreading morphology. This method requires human input, and is therefore inefficient, and also subject to bias. It is also a very coarse classification method. Human observers of dislocation core structures have tended to sort the structures into a small number of bins. For example in HCP metals most references only discuss basal, prismatic, pyramidal, and something along the lines of asymmetric or mixed morphologies [13,17,28,34,35]. This human classification scheme may in fact be glossing over the significance of core structures that do not fit neatly into one of these bins, and/or the importance of intermediate core structures.

Automating the characterization of dislocation core morphologies requires some thought as to how to determine which atoms should be considered to be part of the dislocation core, and to determine how the distribution of core atoms can be converted into a descriptor for the dislocations. One reasonable set of choices is to allow all atoms to contribute to core structure identification and to weight contributions by a function of the atomic strain. Intuitively this makes sense, because a dislocation core is a highly strained region, and thus the atomic strains in the core should be large compared to the surrounding elastically-strained material. The atomic strain may fall off quickly or slowly as a function of distance from the dislocation core, and measuring the rate at which it does could provide an estimate of the dislocation core size. Moreover, considering more-strained atoms to contribute more to the assessment of the dislocation core orientation matches (and formalizes) the existing practice when identifying core structures by eye.

As noted above, two methods for visualizing dislocation core structures are common: the Nye tensor and differential displacement maps. The differential displacement map construction is useful for visualization, but it can be inconvenient choice if one attempts to use it to automate dislocation core identification. For $\langle a \rangle$ -type screw dislocations in HCP metals, at each atom column position there are 6 different vectors connecting to the neighboring columns. The lengths of these vectors are scaled by the relative displacement between the columns. As mentioned earlier, the pattern of displacements is typically classified by eye into one of a small number of categories. While machine learning methods might be used to automate this classification scheme, the necessary automation is not immediately available. Of course, the Nye tensor, the curl of the atomic strain [36], robustly represents the Burgers vector density at each atom position, and can be used to assess differences between dislocation core structures.

In this work, however, an additional dislocation core identification method complementary to both the Nye tensor and the differential displacement map is introduced. This parameter

relies only on the atomic strain computed at a column of atoms. The parameter, denoted as ν , is based on identifying atoms that are near to or beyond elastic instability as predicted by a continuum nonlinear elasticity analysis. Specifically, one sometimes-used definition for a dislocation core is that it is the region in which the stress predicted by continuum linear elasticity theory is greater than the ideal strength of the material [37–39]. The intuition behind this is that in this region linear elasticity theory is certainly no longer applicable, and the material within the region is, at a minimum, nonlinear elastic, and may be, in fact, elastically unstable. This definition is interesting because it suggests that the extent to which an atom is within a dislocation core can be calculated from the strain itself rather than from a derivative of the strain. For the analysis presented here, this choice has the advantage that the stacking faults associated with core dissociation are naturally identified as being within the core of the dislocation, rather than identifying two separate partials with perfect crystal intervening. This might aid in identifying the topological characteristics of the spreading/splitting (if present).

Following the work of de Jong *et al.* [40] and Winter *et al.* [41], the ideal strength of a material (i.e., the elastic limit) can be estimated if one knows the second- and third-order elastic constants (SOECs and TOECs) for the material. Estimates of the ideal strength, and the associated ideal strain, are obtained by finding the eigenvalues of the symmetrized Wallace tensor [42] (Λ), that governs the elastic stability of a crystal under a uniform applied load [43]. Λ is defined in terms of the elastic constants under finite deformation (ECFD), C'_{klmn} , and second Piola-Kirchhoff stress tensor (PKST), τ_{kl} , as

$$\Lambda_{klmn} = C'_{klmn} + \frac{1}{2}(\tau_{km}\delta_{ln} + \tau_{kn}\delta_{lm} + \tau_{lm}\delta_{kn} + \tau_{ln}\delta_{km} - \tau_{kl}\delta_{mn} - \tau_{mn}\delta_{kl}), \quad (1)$$

with δ_{kl} being the Kronecker- δ . As Λ governs the elastic stability of a solid under a uniform applied load, if an eigenvalue of the symmetrized Wallace tensor goes to zero the ideal strength has been reached. The key to estimating ideal strengths within a nonlinear elastic framework is to estimate ECFD and the PKST in terms of an applied strain η , SOECs and TOECs as described in Refs. [40,41]. In theory, the elastic constants used to determine the Wallace tensor should be computed at finite temperature. In practice, the zero temperature values seem to suffice. The values of the elastic constants used in the current work are presented in the Appendix.

This nonlinear elastic model can be applied to aid in understanding the structure of defects in materials as modeled through atomistic simulations. The core region associated with a crystalline defect is often qualitatively described as a region lacking crystallinity. It can be assumed that this is a result of the large strains near the origin of a defect causing the atoms near the defect to rearrange themselves to the point that they no longer correspond to the lattice of the defect-free material. By further assuming that local nonlinear continuum elasticity theory can accurately predict where this instability will occur, atomic strains can be estimated using various methods [44,45], and then used to estimate the eigenvalues of Λ , to evaluate an atom's nearness to a defect core.

Accordingly, for the α th atom in a system, one defines the parameter ν^α :

$$\nu^\alpha = \frac{\min[\text{eig}(\Lambda^{\text{ref}})] - \min[\text{eig}(\Lambda^\alpha)]}{\min[\text{eig}(\Lambda^{\text{ref}})]}, \quad (2)$$

where Λ^{ref} is the symmetrized Wallace tensor for the reference (undeformed) system, and Λ^α is the symmetrized Wallace tensor for atom α in the current configuration of an atomistic simulation. Given that $\min[\text{eig}(\Lambda^{\text{ref}})] > 0$ for a stable reference configuration and $\min[\text{eig}(\Lambda^{\text{ref}})] \geq \min[\text{eig}(\Lambda^\alpha)]$, the parameter $\nu \geq 0$. The inputs required for this calculation are the atomic positions in the current state, a reference (undeformed) lattice, and the second- and third-order elastic constants of the system under no applied stress. Note that as described here, the computation of ν requires no adjustable parameters.

To determine if the ν parameter is useful in practice, we compare it with the established dislocation identification methods of Nye tensor analysis [36] and differential displacement maps [6] for the same dislocation. One test case that is both simple and important is the representation of the ground-state dislocation cores calculated by DFT. A comparison of these between the existing Nye tensor and differential displacement map visualizations and ν is presented in Fig. 1 for the case of the ⟨a⟩-type screw dislocation cores in titanium from Ref. [17].

Another important test case is the performance of this parameter on atomic positions extracted from an MD simulation, because these will have thermal noise. If this parameter is to be used to classify core structures generated by MD simulations, then it must be able to tolerate this noise. An example of this is shown in Fig. 2. As Fig. 2 demonstrates, ν represents the core structure effectively in that it is similar to a plot of the Nye tensor screw component.

In considering the previous description of the ν parameter it is important to note that ν should be considered an indicator of the region's nearness to instability, and not an absolute stability criterion. Note that within the core of the dislocation, the computed strains are often large enough to place the atoms in the unstable range of strains, according to Λ . Clearly, based on the atomic scale calculations, these atoms remain stable in their positions. Also, the assumption of locality is rather strong: instabilities caused by “soft” phonons away from the Γ -point could possibly play a significant role, as is found to be the case in some ideal strength calculations [46]. However, due to the great added complexity in determining the force-constant matrix as a function of strain, and the encouraging results shown in this work (see Sec. III), only elastic instabilities are considered in this method.

It is also noted, as mentioned above, that the elastic instability parameter does not distinguish between different sources of displacements. For example, stacking faults are indicated to be elastically unstable, and appear naturally as part of the dislocation. This can be contrasted with the Nye tensor, which is strictly finite only where there is Burgers vector density. In some situations, such as that described below, it is helpful to have the relevant stacking faults labeled as part of the dislocation (which also includes, of course, the partials).

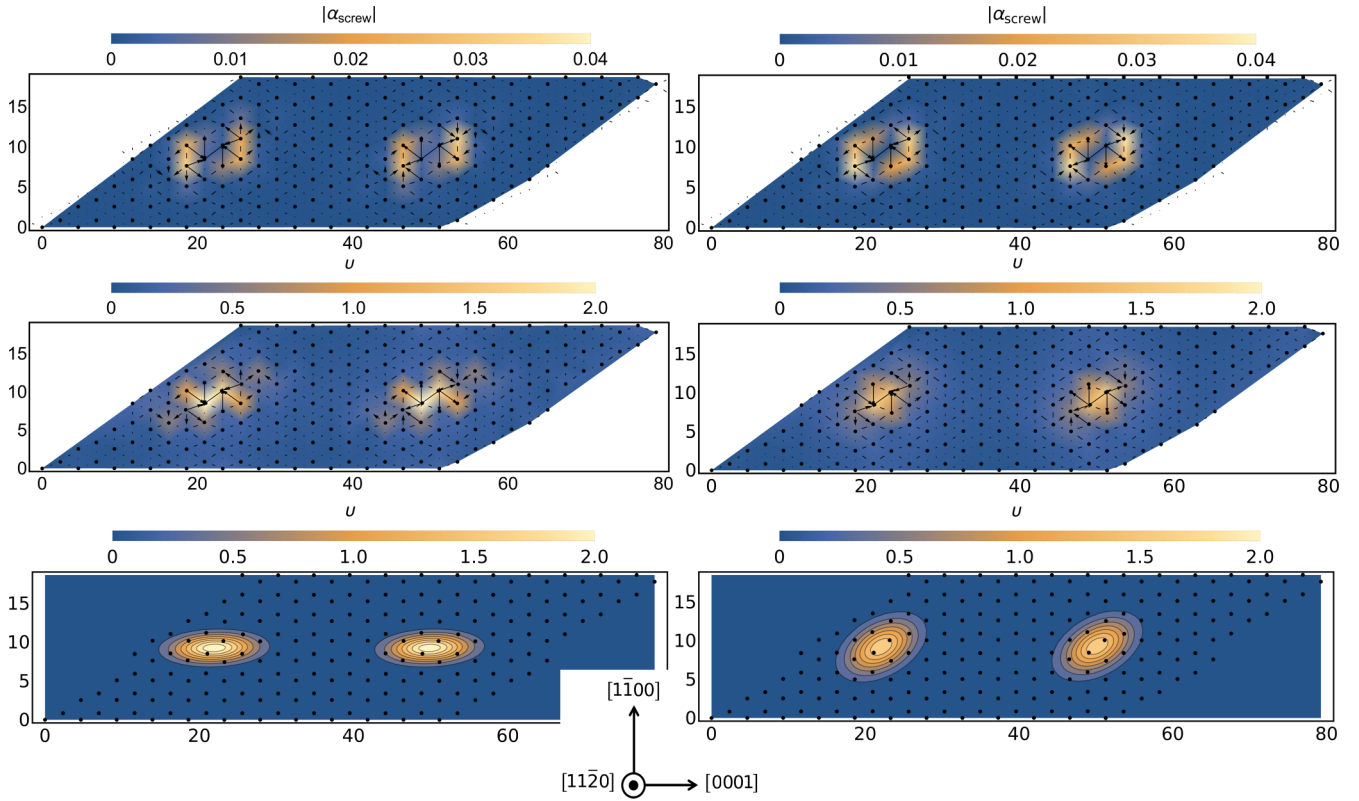


FIG. 1. Nye tensor (in units of \AA^{-1}), elastic instability parameter (dimensionless), and ellipse fitted to Eq. (3) (left) for the unstressed core as predicted by density functional theory and (right) for the core under a compressive stress of 1 GPa along the $[1\bar{1}00]$ direction. From top to bottom in each column is the Nye tensor, the elastic instability parameter, and the fit to the form of Eq. (3). The angles for the ellipses in the two cases are 88° and 61° , respectively (both measured relative to the basal plane).

Taking ν as the choice for weighting the contribution of each atom to the dislocation core, the next step is to choose a method of extracting the relevant dislocation core spreading information, or a descriptor for the core structure. In the present case, we are interested in finding the distribution and evolution in space and time of $\langle a \rangle$ -type screw dislocation core structures in α -Ti. From experience, we know that these tend to be fairly planar and extended along pyramidal and prismatic planes. Therefore, in this study the key parameter of interest is the angle the dislocation core spreading makes with some fixed plane of interest. For example, the basal plane is taken as a reference here, so the prismatic orientation is at 90° and the first-order pyramidal orientations are at 61.5° and 118.5° for the c/a ratio (1.596) of the modified embedded atom method (MEAM) potential of Hennig *et al.* [31] at 0 K. For other problems, completely different features that can be extracted using the ν calculation may be of more interest.

To extract the core orientation the computed values of ν are fitted to a two-dimensional Gaussian function of the form:

$$\nu^{fit}(\xi, \psi) = \max(\nu) \exp[-A(\xi - \xi_0)^2 - B(\xi - \xi_0)(\psi - \psi_0) - C(\psi - \psi_0)^2], \quad (3a)$$

$$A = \frac{\cos^2(\theta)}{2\sigma_1^2} + \frac{\sin^2(\theta)}{2\sigma_2^2}, \quad (3b)$$

$$B = \frac{\sin(\theta)\cos(\theta)}{\sigma_1^2} - \frac{\sin(\theta)\cos(\theta)}{\sigma_2^2}, \quad (3c)$$

$$C = \frac{\sin^2(\theta)}{2\sigma_1^2} + \frac{\cos^2(\theta)}{2\sigma_2^2}, \quad (3d)$$

where $\max \nu$ is fixed to be the maximum computed value for ν , ξ and ψ are the components of position projected onto the plane normal to the dislocation line direction, $\{\xi_0, \psi_0\}$ is the center of the dislocation, θ is the dislocation orientation angle relative to the basal plane, and σ_1 and σ_2 are the magnitudes of the major and minor axes. These allow for definition of the eccentricity of the core (i.e., a characterization of how planar the core structure is) $\mathcal{E} = \frac{\sigma_1}{\sigma_2}$. Viewed as a contour plot the result looks elliptical.

Figure 1 displays the fits to the core structures predicted by DFT for both the unstressed case and the case wherein the core is subjected to a compressive stress of 1 GPa along $[1\bar{1}00]$. Interestingly, the fit for the core dubbed pyramidal in the literature yields an angle of 88 degrees from the basal plane—an angle very near to that expected for the prism spread core. Examination of the Nye tensor plots reveals that the dislocation density is, indeed, not as spread along the pyramidal planes as the differential displacement map seems to indicate. Fitting to an ellipse brings out this behavior. The application of the non-Schmid stress, however, reorients the ellipse, and yields an angle of 61 degrees. Note that the

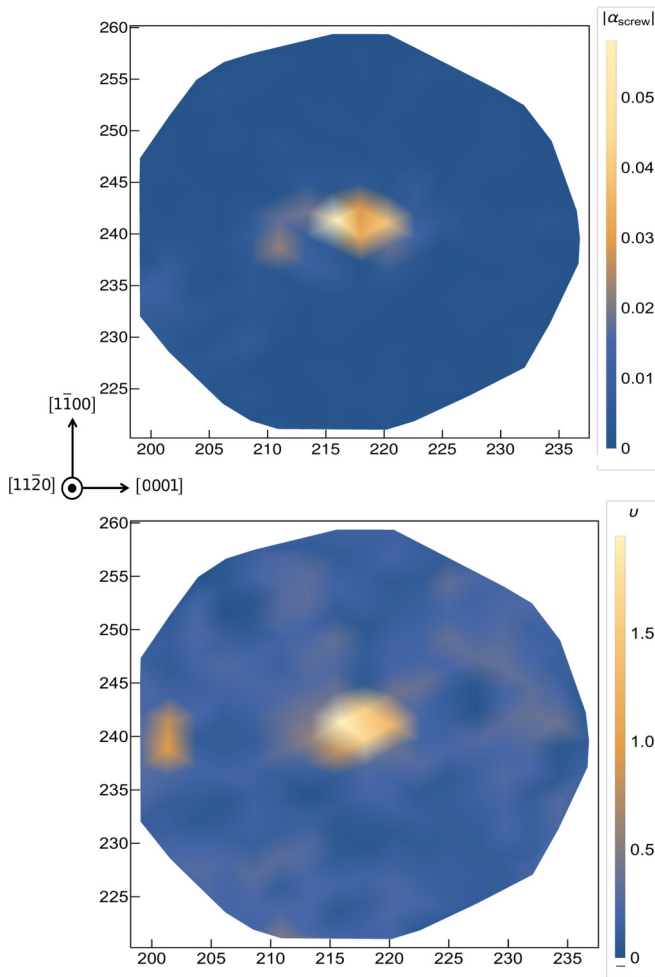


FIG. 2. Top: Nye tensor screw component representation of the sample dislocation core. Bottom: The parameter ν representation of the same dislocation core. This example comes from an MD simulation at 300 K using the MEAM potential for titanium. Lengths are measured in Ångstroms.

changes in core structure between the two stress states are subtle. From the Nye tensor plot, one can clearly see the shift in dislocation density to being more heavily weighted along the pyramidal plane at higher non-Schmid stress. This shift is also obvious in the computation of the elastic instability

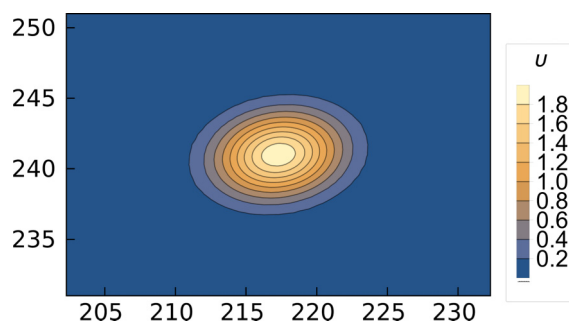


FIG. 3. Fit of Eq. (3) to the parameter ν calculated for the same dislocation core shown in Fig. 2. Lengths are measured in Ångstroms.

parameter. It is more difficult to see the subtle changes in the differential displacement map. This analysis suggests that there is, perhaps, not a single pyramidal core structure, but a continuum of cores defined by subtle variations in core displacements. This observation is supported by the molecular dynamics simulations reported below.

The procedure can also be applied to the cores obtained at temperature, like that in Fig. 2. For this example core, θ is found to be 81.7° , as shown in the fit displayed in Fig. 3 indicating that the dislocation is more near to being spread on the prism plane than being fully spread on the pyramidal plane. \mathcal{E} is 1.51, indicating an extension of the core along the identified direction. Both of these findings match with what we would have determined visually from the Nye tensor shown in Fig. 2.

III. APPLICATION TO $\langle a \rangle$ -TYPE SCREW DISLOCATION CORES IN MD: RESULTS AND DISCUSSION

As discussed in previous literature [17,32,47], the MEAM potential for titanium employed here predicts a prismatic core structure as the ground state for $\langle a \rangle$ -type screw dislocations, which does not agree with DFT calculations (in which a pyramidal core structure is predicted). However, it is also known that there are effects of non-Schmid stresses on the structure of $\langle a \rangle$ -type screw dislocations in Ti as described within the MEAM potential of Hennig *et al.* [31] when a tensile or compressive stress is applied along the $[1\bar{1}00]$ axis. In fact, a non-Schmid stress can induce a transformation of the dislocation core structure from prismatic to pyramidal (based on the differential displacement map). Some interesting aspects of this can now be studied using the approach outlined above. In particular by applying non-Schmid stresses we can study the dislocations with either a prism or pyramidal spread core as the ground state, and compare their dynamics.

To begin these studies, a series of MD simulations using a supercell with dimensions $300 \text{ \AA} \times 325 \text{ \AA}$ on its face and 94 \AA along the dislocation line (i.e., 32 Burgers vectors deep) containing two dislocations arranged in the S configuration [12] were performed using LAMMPS [48]. The data for the individual dislocations are collected and analyzed separately. In these simulations the temperature was in the range 50 to 500 K, and the non-Schmid stress on the $[1\bar{1}00]$ axis was in the range 0 to 1 GPa. Each simulation made use of an $N\sigma T$ ensemble with a Langevin thermostat and Parrinello-Rahman barostat [49], and was run for 100 ps using 1 fs timesteps. The atomic positions were saved every 1 ps, and these were used to generate the dislocation core orientation data. To accelerate data collection, the dislocation extraction algorithm (DXA) [50,51] in OVITO [52] was employed to locate the centers of the dislocations, and ν was only calculated for atoms near to these centers.

ν is calculated for every slice of the supercell (each slice is 1 Burgers vector thick, the minimum repeat length along the dislocation line direction) at each saved timestep, and thus there are nominally 6400 core orientations calculated for each simulation. Unfortunately, not every calculation yields reliable data. The eccentricity of the fitted Gaussian, Eq. (3) used to compute the angle, \mathcal{E} , was used to filter the data set used for further analysis. Orientations corresponding to

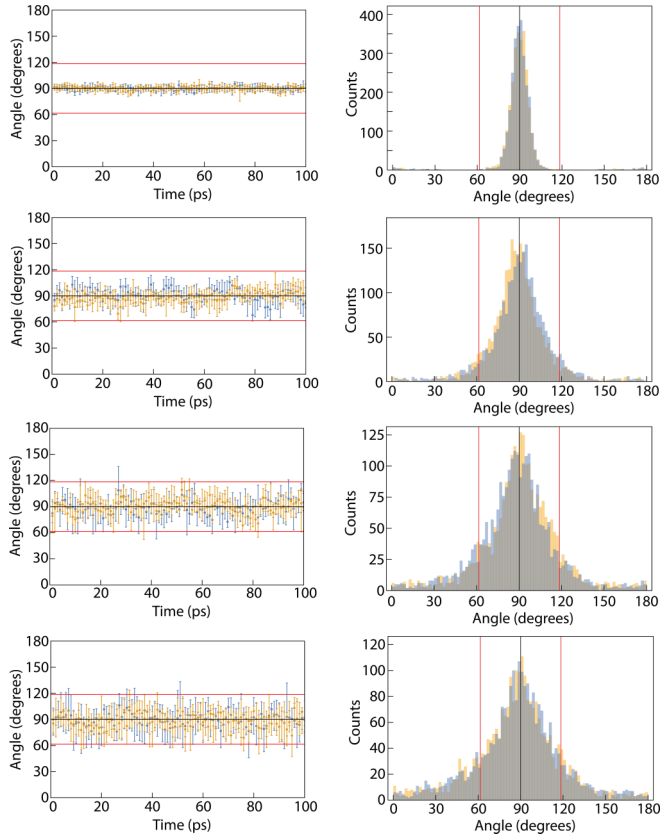


FIG. 4. Core orientations (left) and histograms (right) of all assignable core structure orientations slices for both dislocations in MD simulation at 100 K, 300 K, 400 K, and 500 K (top to bottom) under no applied stress. The black line shows the nominal position of the prismatic orientation and the red lines are the nominal pyramidal orientations.

cores with $1.25 \geq \mathcal{E} \geq 4.00$ were used for the analysis, and those outside of that range were discarded. This was based on a heuristic analysis that eccentricities outside of that range typically correspond to failed convergence of the fit in Eq. (3). It also naturally makes sense that when \mathcal{E} is close to 1 the orientation is not significant, since the core is roughly circular. In the simulations presented here, this typically removes 10–15% of the total data. This neglect of certain configurations of dislocations is reasonable as long as one is careful about the conclusions drawn from the resulting data. In particular, the data provides only an approximate measurement of the relative concentrations of the differing core-spreadings along a single dislocation. The analysis below, then, focuses on key trends and qualitative observations, rather than on a quantitative estimate of the fractions of the core that are of one type versus another.

A. Effects of temperature

As noted above, the simulation cells contain a dislocation dipole, and the data presented here is separated by dislocation. Simulations at 100 K, 300 K, 400 K, and 500 K under no applied stress were each conducted for 100 ps, and the results are summarized in Fig. 4. The following discussion will focus on visualizations using the median, lower quartile and upper

quartile core orientation angles at each timestep as in the left column of Fig. 4, and histograms of the core distributions over the entire simulation as in the right column of Fig. 4. Specifically, at each recorded time step, the median angle value, and the lower and upper quartile core orientations from the segments of each dislocation are recorded as the symbol and the error bars, respectively. Thus, each symbol represents the structure of an entire dislocation (less the slices that could not be quantified with an angle) at the indicated time. The orange symbols correspond to one of the dislocations in the unit cell, the blue symbols correspond to the other.

The histograms in Fig. 4, in contrast, represent the behavior over time of the individual dislocations as they include the angle configuration data from all times (after equilibration) and from all slices of the dislocation that could be assigned an orientation angle. Again, the results for one dislocation are shown in orange, and for the second in blue. When the histograms overlap, they appear gray.

Clearly, as the temperature increases the width of the dislocation core orientation distributions increases significantly. At 100 K virtually all assignable cores are prismatically-oriented, with few outliers further than 10° from the prismatic orientation. At 500 K almost all possible core orientations have at least some representation, and at most timesteps even the median core orientation is at least 10° from prismatic. The increase in the spread of the core orientations within each timestep is also significant. At higher temperatures we find dislocations ranging from prismatic to pyramidal on the same dislocation at the same instant frequently. Another observation is that at higher temperatures the overall orientation of the dislocation changes much more rapidly, i.e., the median core orientation for a dislocation changes from pyramidal to prismatic to the other pyramidal regularly. At 100 K there are none of these changes observed.

These behaviors at elevated temperatures largely match expectations. Note that in all cases, the fitting reveals that there is not a single pyramidal core structure, but rather a range of core structures. Note also that as the temperature increases, the angular range of the cores, as measured by the width of the distribution, is increasing. The increase in the angle with temperature suggests that at higher temperatures, the cores begin to look more frequently like those in Fig. 1(b) than those like Fig. 1(a).

Note that the crystallographic angles describing the relationship between the prism and pyramidal planes do appear special in these distributions. This is one lesson that can be learned from removing the human element of classification and instead looking at algorithmically generated data. The prismatic orientation is the ground state with no applied stress and the pyramidal orientation is accessible within thermal energies (there is a $9 \text{ meV}/b$ potential energy difference [17] under zero stress as modeled within the MEAM potential). It follows that increasing the temperature would allow for significant occupation of the pyramidal structure.

The histograms resulting from higher-temperature simulations indicate that the occupations of orientations varies somewhat smoothly. This is mildly surprising, since up to this point the discussion has revolved around a finite number of possible core structures rather than a continuous distribution of structures. Physically, though, this is reasonable. Interme-

diate core structures are necessary for transitions between primary structures (i.e., prismatic, pyramidal, basal) to occur. Moreover, thermal fluctuations induce variation about a local equilibrium structure, as can be seen in the 100 K distributions that sample primarily prismatic core structure. Given the low potential energy differences between the core structures discussed previously, it is not surprising to conclude that the potential energy landscape is relatively flat and that this leads to the smooth orientation distributions.

B. Effects of non-Schmid stress

By applying stresses with zero resolved shear stress on $\langle a \rangle$ -type screw dislocations, the ground-state core structure of these dislocations in the MEAM potential can be changed. More specifically, when a large compressive stress is applied on the $[1\bar{1}00]$ axis the equilibrium core structure changes from prismatic to pyramidal. The ν parametrization can be used to investigate the pressure at which this transition occurs. Consider, then, the series of simulations with different applied stresses on the $[1\bar{1}00]$ axis, all at 100 K (Fig. 5). This temperature was chosen because Fig. 4 indicates that there will be minimal spread of the orientations due to thermal fluctuations, and thus it will be simple to assess which core structure is favored.

As discussed previously, the core structure under no applied stress is purely prismatic with very little deviation. With 125 MPa compression applied on the $[1\bar{1}00]$ axis, evidence of a small number of excursions toward pyramidal core structures are observed. Further increasing the compression to 200 MPa, the dislocations spend approximately equal time in prismatic and pyramidal orientations. This, roughly speaking, is the transition pressure at 100 K. It is clear that the transition from one core structure to the other is not sharp (in this supercell), which makes determining the pressure at which it occurs inexact. In the histogram from the 200 MPa, 100 K, simulation one can see that the individual histograms are asymmetrically distributed about the prism core orientation, indicating that the pyramidal orientations are occupied to a greater extent than simply as variations about the prismatic orientation. Further increasing the compression to 500 MPa results in only pyramidal core structures. With this simulation it was somewhat fortunate that the two dislocations happened to occupy opposite pyramidal orientation—as mentioned before, the dislocations sample the same distribution so there is no reason to expect this. This results in a histogram that neatly shows the orientations of the two pyramidal structures occupied at this temperature and pressure. At the highest compressive stress simulated (1 GPa), the dislocations happened to select the same pyramidal plane and not transition to any other structures, and thus the distributions overlap. If one compares the histograms resulting from the 500 MPa and 1 GPa simulations quite carefully, then it can be observed that the peaks of the distributions are slightly different. With 500 MPa compression applied the lower-angle pyramidal orientation peak is at 71.5° , while under 1 GPa it is at 68.0° , which is closer to the ideal pyramidal orientation (and similar to the orientation calculated for the DFT ground-state under the same non-Schmid stress). The distribution corresponding to an applied compression of 250 MPa (not shown), results in

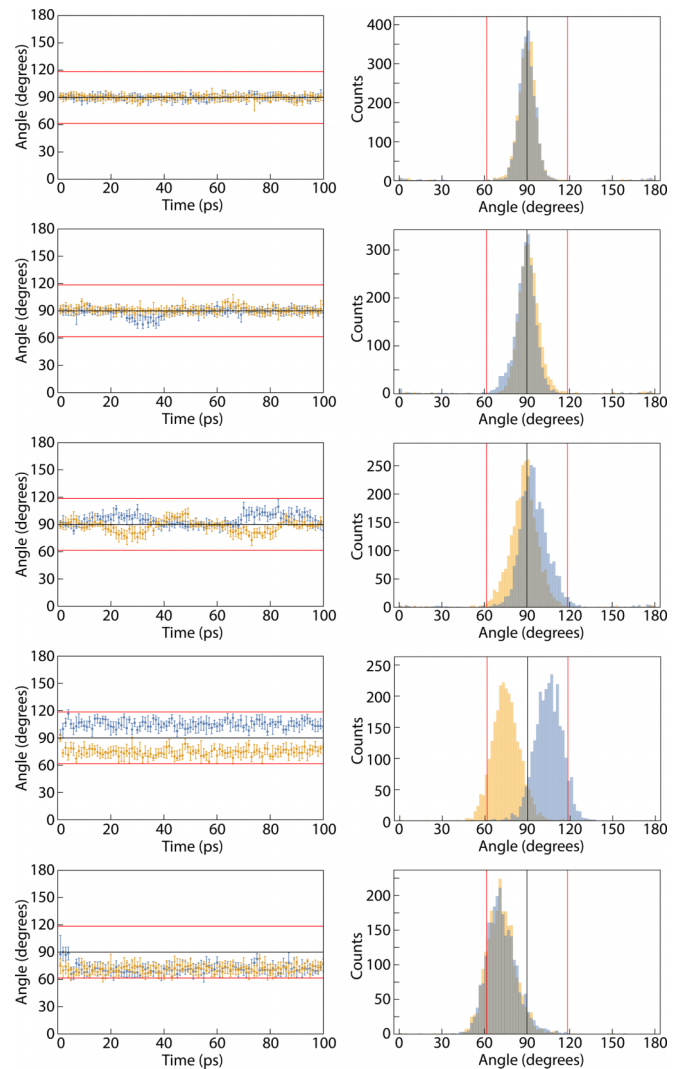


FIG. 5. Core orientations (left) and histograms (right) of all core structure orientations slices for both dislocations in MD simulation at 0 MPa, 125 MPa, 200 MPa, 500 MPa, and 1 GPa (top to bottom) non-Schmid stress applied on the $[1\bar{1}00]$ axis at 100 K. The black line indicates the prismatic orientation and the red lines the pyramidal orientations.

pyramidal cores peaked at 74.6° , which continues this trend. These are substantial differences in core orientations, and the trend implies that the effect of non-Schmid stresses goes beyond selecting the degree to which the prismatic and pyramidal orientations are occupied; in fact, they also influence the preferred configuration of pyramidal core structures.

Given the significant changes induced by the non-Schmid stresses on the dislocation core structures, one would anticipate strong effects on dislocation slip behavior and thus on plastic deformation. Specifically, in light of the core structure-based explanation for the locking-unlocking mechanism proposed by Clouet *et al.* [13], the expected behavior is that under zero non-Schmid stress the dislocations should be able to slip easily on the prismatic plane (known to be the dominant slip plane in titanium), whereas under large non-Schmid stresses that induce the pyramidal core orientation slip should be much more difficult. In other words, it is expected

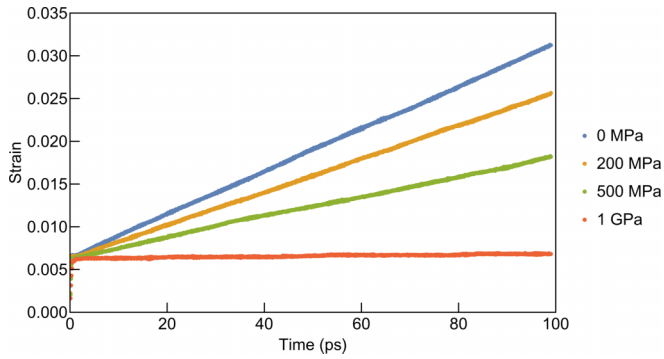


FIG. 6. Shear strain vs time for MD simulations with 200 MPa shear stress for prismatic slip and 0 MPa, 200 MPa, 500 MPa, and 1 GPa non-Schmid compression along the $[1\bar{1}00]$ axis applied at 100 K.

that the dislocation cores will be unlocked under no applied compression on the $[1\bar{1}00]$ axis, and locked under 500 MPa and 1 GPa compression on the same axis, based on the orientation distributions shown in Fig. 5. For intermediate stresses for which both prismatic and pyramidal cores are represented we expect some slip to occur, but less than for the totally unlocked state.

To investigate these predictions, we performed simulations very similar to the previous set described above, but with a shear stress of 200 MPa oriented with the maximum resolved shear stress on the prismatic plane applied in addition to the non-Schmid stresses. A plot of shear strain versus time for simulations with 0 MPa, 200 MPa, 500 MPa, and 1 GPa non-Schmid stress applied at 100 K is shown in Fig. 6.

Examining the strain data in Fig. 6, it is evident that the predictions largely held true. Slip occurs readily when no non-Schmid stress is applied—the unlocked configuration—and with increasing compression on the $[1\bar{1}00]$ axis the strain decreases. When 1 GPa compression is applied—the locked configuration—the dislocations hardly slipped at all. At 200 MPa, substantial slip occurred because the prismatic orientation is accessible. The only surprising simulation is that under 500 MPa compression. Under these conditions the core is almost entirely pyramidally oriented when there is no shear applied, so one anticipates little or no prismatic slip to occur. However, it is now clear that this stress is not high enough to make the prismatic orientation inaccessible at 100 K, and thus under applied shear stress the cores were able to transform into the prismatic configuration and accommodate slip. One can compute the core structure distributions during slip exactly as at rest, and thus verify that the differences in strain are in fact due to the amount of locking of the dislocation cores. The core structure distributions corresponding to the simulations under shear stress at 100 K are shown in Fig. 7.

It is clear that the greater the fraction of the dislocation cores that are oriented along the prismatic plane, the greater the degree of prismatic slip. It is also plain that under 500 MPa and 1 GPa compression the dislocation cores still have a strong tendency toward pyramidal orientation, which is what is expected based on the calculations with no shear stress applied. However, the key difference between these two stress states is the accessibility of the prismatic configuration. At

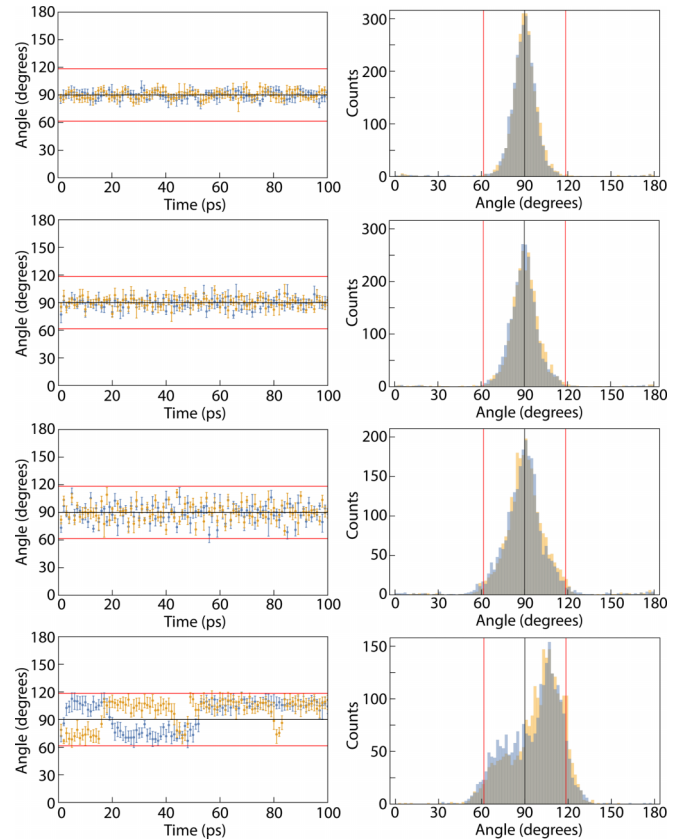


FIG. 7. Core orientations (left) and histograms (right) of all core structure orientations slices for both dislocations in MD simulation with 200 MPa shear stress for prismatic slip and 0 MPa, 200 MPa, 500 MPa, and 1 GPa (top to bottom) non-Schmid stress applied on the $[1\bar{1}00]$ axis at 100 K. The black line indicates the prismatic orientation and the red lines the pyramidal orientations.

500 MPa non-Schmid stress, the distribution of dislocations becomes centered on the prism orientation, but the tails extend to the pyramidal configurations. The dislocations display many transformations between prism and the two pyramidal orientations, as can be seen in the quartile representation which shows frequent switching back and forth across the prismatic line. However, under 1 GPa compression the prismatic orientation is more rarely seen, and the distribution of cores assumes a slight bimodal character. There are only a small handful of slip events observable in Fig. 6 for this stress state, and each of them corresponds to one of the rare occasions that a dislocation core orientation is prismatic. These unlocking events are short-lived, and the cores rapidly return to one or the other of the pyramidal configurations. This behavior is what one might expect based on the locking-unlocking model formulated by Farenc *et al.* [30] and as modeled by Clouet *et al.* [13].

The potential of the dislocations to display the locking-unlocking mechanism due to core structure reorientation can be made more evident by comparing the dislocation core configurations with the positions of the dislocations during the simulation at 1 GPa compression and 200 MPa shear stress at 100 K. The dislocation center positions is a convenient byproduct of using DXA to locate the dislocations as a pre-

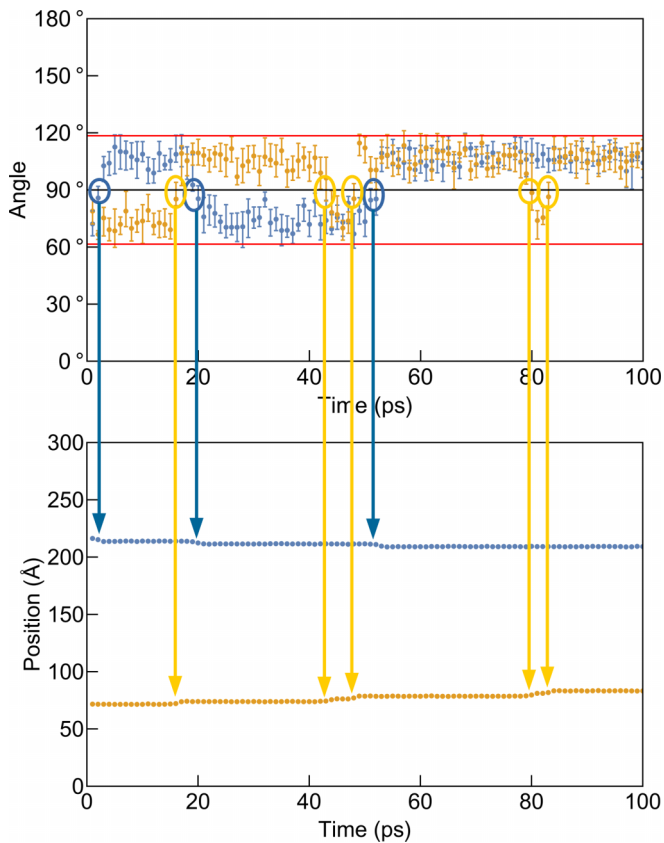


FIG. 8. (Top) Dislocation core orientations during a MD simulation at 1 GPa compression and 200 MPa shear stress at 100 K. (Bottom) Dislocation centroid positions parallel to the $[0001]$ axis during the same simulation. Excursions of the core structure into the prismatic configuration are highlighted, and the correspondence between these and slip steps of the dislocations shown.

processing step during calculation of ν . This comparison is shown in Fig. 8, and it is clear that every movement of the dislocations along the prismatic plane corresponds to a brief unlocking of the dislocation core structure. It is noted that the movements observed here are between individual Peierls valleys and that the dislocations move from one Peierls valley to the next in discrete jumps. (In two instances, there are two events spaced within 10 ps of one another, which may indicate some correlation between them that could lead to longer range motion.) This motion is, thus, not the equivalent of the “jerky” glide seen in the experiments. However, the Peierls mechanism can lead to jerky glide through the nucleation of multikinks [53]. In short, the nucleation of multikinks will lead to large scale motion of the dislocation that is arrested, ultimately, when the multikinks all annihilate at grain boundaries or with opposite signed kinks. It is possible, then, that the short repeat length of the dislocations ($32b$) is the reason dislocations do not propagate more than one or two Peierls valley in an instance. The size of the dislocations studied here may be such that multikinks spanning two or more Peierls valleys cannot form.

As the temperature increases to 300 K, the behavior of the dislocations remains consistent with the behavior observed at

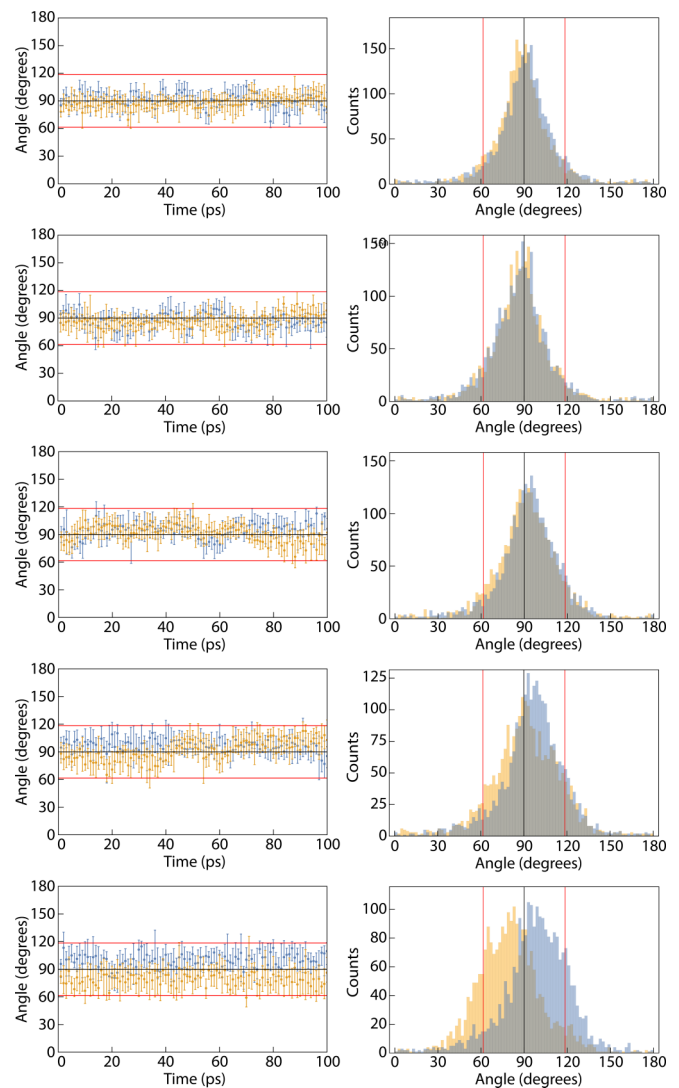


FIG. 9. Core orientations (left) and histograms (right) of all core structure orientations slices for both dislocations in MD simulation at 0 MPa, 125 MPa, 200 MPa, 500 MPa, and 1 GPa (top to bottom) non-Schmid stress applied on the $[1\bar{1}00]$ axis at 300 K. The black line indicates the prismatic orientation and the red lines the pyramidal orientations.

100 K. The core structure angles and distributions without shear stress applied, to parallel Fig. 5, are shown in Fig. 9.

Examination of Fig. 9 yields many of the expected observations, as well as a more subtle, interesting finding. First, the anticipated: For all stress states, the variation in the core orientations is greater at 300 K than at 100 K. This is true both in terms of the widths of the quartiles at each step, and the variation in the median orientations from step to step. This is a straightforward effect of temperature. Higher temperature induces broader distributions of the occupied orientations. A related effect is that the dislocations change their overall orientations more frequently. For example, at 100 K and 500 MPa compression the dislocations settled into pyramidal orientations and did not change to prismatic or the other pyramidal spreading. At 300 K and 500 MPa, a number of reorientations can be observed. Given the findings from the

simulations under shear stress, this suggests that there should be somewhat more slip at 300 K under the larger compressions than there is at 100 K. This would be in line with previous predictions based on a dislocation core structure explanation for the locking-unlocking mechanism [13].

However, comparing the simulations with 0 MPa, 125 MPa, and 200 MPa compression at 300 K with the same applied stresses at 100 K, it appears that at higher temperature there is less occupation of prismatic core structures. This is true not just in the sense of greater fluctuation away from these states (which certainly accounts for some of the difference) but also in the locations of the medians. In fact while at 100 K compression of 200 MPa is found to be the transition pressure, at 300 K there are almost no prismatically oriented median structures at this pressure. This suggests that the transition pressure is reduced at higher temperature. Another way of stating this is that the pyramidal orientations are favored by higher temperature, which implies that these are higher-entropy structures. Calculations on the temperature-dependence of dislocation core structures in semiconductors suggests that in that case vibrational entropy plays an important role in the dislocation structural properties at high temperatures [54] and that configurational entropy can complicate the structures [19,25]. However, the authors are not aware of any literature discussing entropy of competing dislocation core structures in metals. Even when high-temperature effects on core structure are discussed, the entropy of the structures is assumed to be the same [55].

This increase in pyramidal occupations at higher temperatures implies another effect on the dislocation dynamics. Increasing the temperature can decrease the strain rate for a given stress. Certainly at 500 MPa or 1 GPa compression it is expected that the increased accessibility of the prismatic configuration will lead to easier prismatic slip. At 0 MPa compression, though, the core structure is always prismatically oriented at 100 K, but at 300 K there is significant pyramidal orientation occupation. The portions of the core that transition to the pyramidal spreading serve as weak pinning points for the dislocation, and act as sources of drag. Since their number increases with temperature, the dislocations move more slowly at higher temperature. To discover whether this is the case, MD simulations under 200 MPa shear strain at 300 K were carried out and the resulting strains plotted in Fig. 10.

Clearly, Fig. 10 demonstrates that 300 K is sufficient temperature to unlock the dislocations under 1 GPa compression. It is also plain to see that the differences in strain between the different non-Schmid stress simulations are much smaller at 300 K than at 100 K. What cannot be seen easily by eye is that the plastic strain under 0 MPa compression at 300 K is lower than that at 100 K: 2.01% versus 2.45%. This is consistent with the predictions made above.

There are implications of these observations for the dynamics of the $\langle a \rangle$ -type screw dislocations in some HCP metals. It is clear that dislocations that are predominantly pyramidally spread display enhanced mobility with increasing temperatures, whereas dislocations predominantly spread on prism planes display reduced mobility with increasing temperature. It is also interesting to note that the predominant structure of the dislocation may change with increasing temperature and/or application of non-Schmid stresses (and perhaps, glide

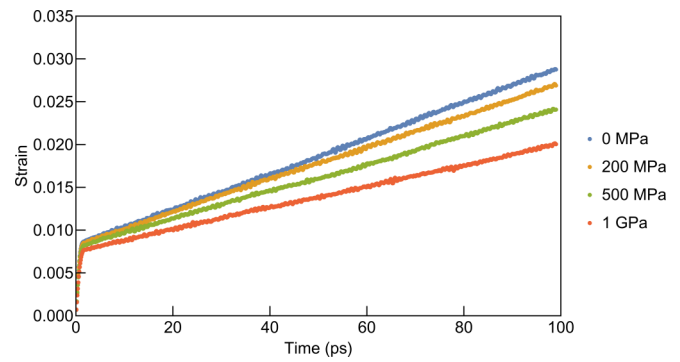


FIG. 10. Shear strain vs time for MD simulations with 200 MPa shear stress for prismatic slip and 0 MPa, 200 MPa, 500 MPa, and 1 GPa non-Schmid compression along the $[1\bar{1}00]$ axis applied at 300 K.

stresses too). A dislocation core switching transition, in which the predominant core structure changes morphology with increasing temperature, could influence the overall slip morphology. For example, prism glide might switch from smooth, perhaps sluggish motion, to a thermally activated Peierls barrier dominated while increasing the propensity for cross-slip (and consequently decreasing slip planarity). The influence of non-Schmid stresses on this transition could lead to situations in which the dynamics of nominally identical dislocations, or even portions of the same dislocation, are markedly different due to differing local stress states.

While this study employs the MEAM potential designed to represent Ti, the general picture that emerges of the dynamics of $\langle a \rangle$ -type screw dislocations is, perhaps, more broadly applicable. It has already been suggested that for Zr, the $\langle a \rangle$ -type screw dislocations are spread primarily on prismatic planes at $T = 0$ K. However, the difference in core energy between the prism plane and pyramidal plane spreading is approximately $12 \text{ meV}/b$ [13]. For the MEAM potential for Ti, this energy difference is $9 \text{ meV}/b$, so the properties of Zr will be similar to those predicted by the MEAM potential for Ti without the application of a non-Schmid stress. One expects the cores of dislocations in Zr to fluctuate, leading to increased drag with increasing temperature. One also expects that the $\langle a \rangle$ -type screw dislocation cores in Zr could undergo a morphological transition with increasing temperature that would lead to thermally-activated dislocation motion at higher temperatures. In their ground state, $\langle a \rangle$ -type screw dislocations in Mg are dissociated into Shockley partials, so their dynamics will differ from that studied here. However, similar methods could be applied to study those dislocations as well.

IV. CONCLUSIONS

Simulations that enable the exploration of the dislocation core morphology for the $\langle a \rangle$ -type screw dislocations in α -Ti have been developed and analyzed. The analysis was aided by the introduction of a parameter (ν) that can be used to gauge how near an atom is to elastic instability. This parameter is used to quantitatively extract structural features of the core spreading of the $\langle a \rangle$ -type screw dislocations in Ti as represented by a MEAM potential, most notably the angle the

TABLE I. Elastic constants for the MEAM potential under no applied stress at 0 K.

C_{11}	174 GPa
C_{12}	95 GPa
C_{13}	72 GPa
C_{33}	188 GPa
C_{44}	58 GPa
C_{111}	-1850 GPa
C_{112}	-965 GPa
C_{113}	-443 GPa
C_{123}	-628 GPa
C_{133}	-292 GPa
C_{144}	-129 GPa
C_{155}	170 GPa
C_{166}	-507 GPa
C_{333}	-93.5 GPa
C_{355}	117 GPa

predominant plane of spreading makes with the basal plane, the angle θ . Molecular dynamics simulations for a classical potential model of HCP Ti were performed over a range of temperatures and applied stress—both non-Schmid and with shear stress oriented for prismatic slip—and core orientation distributions were calculated using the developed framework.

This data illustrates a number of facts about the dependence of dislocation orientations on temperature and stress state. With increasing temperature, the width of orientation distributions is increased as higher-energy core structures become thermally occupied. With increasing compressive stress applied along the $[1\bar{1}00]$ axis, the dislocation core orientations shift from prismatic to pyramidal, but there is apparently no sharp transition between these states for this system size. Interestingly, for this MEAM potential the transition pressure from the prismatic to pyramidal core structure is lowered by increased temperature, implying that higher temperatures favor pyramidal orientations. This implies that these orientations have higher entropy than the prismatic orientation,

suggesting the possibility of a dislocation core morphology switching transition.

In molecular dynamics simulations with shear stress applied to induce prismatic slip, the influence of the cores spreading is apparent. Under 1 GPa of compressive non-Schmid stress at 100 K, every slip step of the dislocations can be shown to correspond to an unlocking event. At 300 K and the same stress, slip is substantially easier because the prismatic core structure is thermally accessible. However, the strain rate under no compression is reduced in these simulations by increasing the temperature, because this leads to a higher pyramidal core structure occupation.

The implications for the dynamics of the $\langle a \rangle$ -type screw dislocations in HCP Ti are discussed. It is noted that dislocation core morphological switching, induced either by temperature or stress (or both), implies significant changes in the temperature dependence of the dislocation dynamics, including the potential to alter observed slip morphologies.

ACKNOWLEDGMENTS

The authors thank Siying Li for her careful read of the manuscript. The authors gratefully acknowledge funding from the U.S. Office of Naval Research under Grants No. N00014-16-1-2304, No. N00014-19-1-2376 (M.P. and M.A.), and No. N00014-16-S-BA10 (I.W. and D.C.C.). This research used the Savio computational cluster resource provided by the Berkeley Research Computing program at the University of California, Berkeley (supported by the UC Berkeley Chancellor, Vice Chancellor for Research, and Chief Information Officer). This work made use of computational resources provided by the Extreme Science and Engineering Discovery Environment (XSEDE), which is supported by National Science Foundation under Grant No. ACI-1053575.

APPENDIX: ELASTIC CONSTANTS

The elastic constants under no applied load used for the calculation of elastic constants under finite deformation were calculated for the MEAM potential used here at $T = 0$ K. These are summarized in Table I.

-
- [1] R. Peierls, *Proc. Phys. Soc.* **52**, 34 (1940).
 [2] F. R. N. Nabarro, *Proc. Phys. Soc.* **59**, 256 (1947).
 [3] R. Chang and L. J. Graham, *Physica Status Solidi (b)* **18**, 99 (1966).
 [4] R. Chang, *Philos. Mag. J. Theor. Exper. Appl. Phys.* **16**, 1021 (1967).
 [5] M. S. Duesbery, *Philos. Mag. J. Theor. Exper. Appl. Phys.* **19**, 501 (1969).
 [6] V. Vitek, R. C. Perrin, and D. K. Bowen, *Philos. Mag.* **21**, 1049 (1970).
 [7] V. Vitek, *Cryst. Lattice Defects* **5**, 1 (1974).
 [8] L. Romaner, C. Ambrosch-Draxl, and R. Pippan, *Phys. Rev. Lett.* **104**, 195503 (2010).
 [9] D. J. H. Cockayne and V. Vitek, *Physica Status Solidi (b)* **65**, 751 (1974).
 [10] Y. Minonishi, S. Ishioka, M. Koiwa, S. Morozumi, and M. Yamaguchi, *Philos. Mag. A* **43**, 1017 (1981).
 [11] M. H. Liang and D. J. Bacon, *Philos. Mag. A* **53**, 181 (1986).
 [12] E. Clouet, *Phys. Rev. B* **86**, 144104 (2012).
 [13] E. Clouet, D. Caillard, N. Chaari, F. Onimus, and D. Rodney, *Nat. Mater.* **14**, 931 (2015).
 [14] P. Kwasniak and H. Garbacz, *Acta Mater.* **141**, 405 (2017).
 [15] P. Kwasniak and E. Clouet, *Scr. Mater.* **162**, 296 (2019).
 [16] P. Kwasniak and E. Clouet, *Acta Mater.* **180**, 42 (2019).
 [17] M. Poschmann, M. Asta, and D. C. Chrzan, *Modell. Simul. Mater. Sci. Eng.* **26**, 014003 (2018).
 [18] D. C. Chrzan, M. Poschmann, I. S. Winter, and M. Asta, *Phys. Rev. Materials* **6**, 013604 (2022).
 [19] A. Valladares and A. P. Sutton, *J. Phys.: Condens. Matter* **17**, 7547 (2005).

- [20] G. Lu, N. Kioussis, V. V. Bulatov, and E. Kaxiras, *Phys. Rev. B* **62**, 3099 (2000).
- [21] P.-A. Geslin and D. Rodney, *Phys. Rev. B* **98**, 174115 (2018).
- [22] J. Bennetto, R. W. Nunes, and D. Vanderbilt, *Phys. Rev. Lett.* **79**, 245 (1997).
- [23] X. Blase, K. Lin, A. Canning, S. G. Louie, and D. C. Chrzan, *Phys. Rev. Lett.* **84**, 5780 (2000).
- [24] N. Lehto and S. Öberg, *Phys. Rev. Lett.* **80**, 5568 (1998).
- [25] S. Beckman and D. C. Chrzan, *Phys. B: Condens. Matter* **340–342**, 990 (2003).
- [26] L. Pizzagalli, J. Godet, and S. Brochard, *Phys. Rev. Lett.* **103**, 065505 (2009).
- [27] P. Kwasniak, H. Garbacz, and K. J. Kurzydowski, *Acta Mater.* **102**, 304 (2016).
- [28] T. Tsuru and D. C. Chrzan, *Sci. Rep.* **5**, 8793 (2015).
- [29] S. Farenc, D. Caillard, and A. Couret, *Acta Metall. Mater.* **41**, 2701 (1993).
- [30] S. Farenc, D. Caillard, and A. Couret, *Acta Metall. Mater.* **43**, 3669 (1995).
- [31] R. G. Hennig, T. J. Lenosky, D. R. Trinkle, S. P. Rudin, and J. W. Wilkins, *Phys. Rev. B* **78**, 054121 (2008).
- [32] M. Poschmann, M. Asta, and D. C. Chrzan, *Comput. Mater. Sci.* **161**, 261 (2019).
- [33] J. Nye, *Acta Metall.* **1**, 153 (1953).
- [34] S. Rao, A. Venkateswaran, and M. Letherwood, *Acta Mater.* **61**, 1904 (2013).
- [35] N. Tarrat, M. Benoit, D. Caillard, L. Ventelon, N. Combe, and J. Morillo, *Modell. Simul. Mater. Sci. Eng.* **22**, 055016 (2014).
- [36] C. S. Hartley and Y. Mishin, *Acta Mater.* **53**, 1313 (2005).
- [37] D. C. Chrzan, M. P. Sherburne, Y. Hanlumuang, T. Li, and J. W. Morris, *Phys. Rev. B* **82**, 184202 (2010).
- [38] C. A. Sawyer, J. W. Morris, and D. C. Chrzan, *Phys. Rev. B* **87**, 134106 (2013).
- [39] I. S. Winter, M. Poschmann, T. Tsuru, and D. C. Chrzan, *Phys. Rev. B* **95**, 064107 (2017).
- [40] M. De Jong, I. Winter, D. C. Chrzan, and M. Asta, *Phys. Rev. B* **96**, 014105 (2017).
- [41] I. S. Winter, M. de Jong, J. Montoya, E. Rothchild, and D. C. Chrzan, *Phys. Rev. Mater.* **3**, 113608 (2019).
- [42] D. Wallace, *Thermodynamics of Crystals*, Dover Books on Physics (Dover Publications, Mineola, NY, 1998).
- [43] W. Morris Jr and C. R. Krenn, *Philos. Mag. A* **80**, 2827 (2000).
- [44] M. L. Falk and J. S. Langer, *Phys. Rev. E* **57**, 7192 (1998).
- [45] P. M. Larsen, S. Schmidt, and J. Schiøtz, *Modell. Simul. Mater. Sci. Eng.* **24**, 055007 (2016).
- [46] D. M. Clatterbuck, C. R. Krenn, M. L. Cohen, and J. W. Morris, *Phys. Rev. Lett.* **91**, 135501 (2003).
- [47] M. Ghazisaeidi and D. R. Trinkle, *Acta Mater.* **60**, 1287 (2012).
- [48] S. Plimpton, *J. Comput. Phys.* **117**, 1 (1995).
- [49] M. Parrinello and A. Rahman, *J. Appl. Phys.* **52**, 7182 (1981).
- [50] A. Stukowski and K. Albe, *Modell. Simul. Mater. Sci. Eng.* **18**, 085001 (2010).
- [51] A. Stukowski, V. V. Bulatov, and A. Arsenlis, *Modell. Simul. Mater. Sci. Eng.* **20**, 85007 (2012).
- [52] A. Stukowski, *Modell. Simul. Mater. Sci. Eng.* **18**, 015012 (2010).
- [53] T. Suzuki and H. Koizumi, *Philos. Mag. A* **67**, 1153 (1993).
- [54] C. R. Miranda, R. W. Nunes, and A. Antonelli, *Phys. Rev. B* **67**, 235201 (2003).
- [55] Y. Jiang, R. Wang, and S. Wang, *Philos. Mag.* **96**, 2829 (2016).